# Varying shell gap and deformation in $N\sim 20$ unstable nuclei studied by the Monte Carlo shell model

Yutaka Utsuno,[1,2] Takaharu Otsuka,[1,2] Takahiro Mizusaki,[1] and Michio Honma[3]
[1]*Department of Physics, University of Tokyo, Hongo, Tokyo 113-0033, Japan*
[2]*RIKEN, Hirosawa, Wako-shi, Saitama 351-0198, Japan*
[3]*Center for Mathematical Sciences, University of Aizu, Tsuruga, Ikki-machi Aizu-Wakamatsu, Fukushima 965-8580, Japan*
(Received 17 February 1999; revised manuscript received 30 June 1999; published 8 October 1999)

The structure of neutron-rich nuclei in the $N\sim 20$ region is studied by the Monte Carlo shell model based on the quantum Monte Carlo diagonalization method. We present a comprehensive description of even-even isotopes of O, Ne, Mg, and Si. It is demonstrated that, for different nuclei, various particle-hole excitations from the $sd$ to $pf$ shell are mixed in different ways, producing distinct effects sometimes, for instance, in $^{28}$Ne. The monopole interaction is examined and modified, resulting in the shell gap changing from nucleus to nucleus. The drip line of O isotopes is then reproduced. The interplay between the $T=0$ and $T=1$ monopole interactions is discussed from the viewpoint of the potential energy surface and the effective single-particle energy. The extension of the neutron drip line of Ne isotopes is explained, and the boundary of the ''island of inversion'' is shown to be rather indistinct. [S0556-2813(99)00211-3]

PACS number(s): 21.60.Cs, 21.60.Ka, 27.30.+t

## I. INTRODUCTION

The shell gap and deformation are two among the most predominant and interesting features of nuclei. These properties are considered to be understood to a large extent for low-lying states of stable nuclei. However, the situation seems to be quite different in unstable nuclei. Neutron-rich unstable nuclei with $N\sim 20$ constitute a good example, as suggested by Thibault *et al.* [1]. In some of such nuclei, extra binding energy is gained by the deformation associated with the particle-hole excitation across the $N=20$ shell gap. The evidence for this structure is clearly seen in $^{32}$Mg from the observed excitation energy [2] and the $B(E2)$ value [3].

If a nucleus gains binding energy through the deformation, the drip line extends farther from the one expected by the closed shell. Recent experiments at GANIL [4,5], MSU [6], and RIKEN [7] show that, although $^{26}$O and $^{28}$O are both unstable for the particle decay, the heaviest Ne isotope jumps at least to $N=22$ [4,8].

Therefore, it is of great interest to study whether or not the binding energies, the level schemes, and the $E2$ properties can be described in a single framework for both stable and unstable nuclei in this region. There have been several theoretical studies on certain nuclei in this region, for instance, using the Skyrme Hartree-Fock approach [9] and the shell-model calculations including the $pf$ shell [10–14]. Such conventional shell-model calculations [10–12,14] were obliged to truncate configurations even within the given shell(s) because of the limitation of the manageable dimension, and some of them [11,14] did not take into account the mixing between the normal and intruder configurations. In this paper, we report on the structure of unstable even-even nuclei in the $N\sim 20$ region from O to Si in terms of the Monte Carlo shell model (MCSM) based on the quantum Monte Carlo diagonalization (QMCD) method [15–18], which can be characterized as the shell model with *importance truncation* [19]. The variation of the shell gap and deformation as functions of $N$ and $Z$ will be of major interest. In the MCSM, we do not restrict the number of particle-hole excitations, and the normal and intruder configurations are mixed naturally. It may be worth mentioning that, because of prohibitively large dimensions in conventional shell-model calculations, physical quantities such as energy levels and $E2$ matrix elements have been calculated in this work for the first time without particle-hole truncations from the $N=20$ core, except for O isotopes. Note that the feasibility of the MCSM calculation has been confirmed in the $pf$-shell region [17,18], where the largest $m$-scheme dimension becomes more than a billion.

The paper is organized as follows. First we present the model space and the effective interaction in Sec. II. We show details of the calculations, including how to treat the spurious center-of-mass motion in Sec. III. The $T=1$ part of the interaction is studied in Sec. IV by comparing the experimental and theoretical two-neutron separation energies, energy levels, and $B(E2)$ values of O isotopes. In Sec. V, the results by the MCSM are shown for Ne, Mg, and Si isotopes, and these results are analyzed in terms of the potential energy surface and effective single-particle energy. The importance of mixing of different particle-hole configurations from the $N=20$ magic core is discussed in Sec. VI. Finally, we summarize the work in Sec. VII.

## II. MODEL SPACE AND EFFECTIVE INTERACTION

In this section, we describe the model space and the effective interaction used in the present study. One of the main purposes of this paper is to examine the persistence and the effects of the shell gap at $N=20$. For this purpose, not only the $sd$ shell but also at least part of the $pf$ shell should be included as orbits where nucleons are active. Thus, assuming that $^{16}$O is an inert core, we adopt the $0f_{7/2}$ and $1p_{3/2}$ orbits as valence orbits as well as the $sd$ shell, as taken in Refs. [10,12].

The effective interaction used here consists basically of

 

three parts as shown below. The $sd$-shell part is the USD interaction [20], where the two-body matrix elements have been fitted so as to reproduce the structure of stable nuclei in the $sd$-shell region. The $pf$-shell part is the Kuo-Brown (KB) interaction [21], which is obtained from the renormalized $G$ matrix. The cross-shell part is the one used in Ref. [22], which is based on the Millener-Kurath (MK) interaction [23]: the eight two-body matrix elements of $\langle 0f_{7/2}0d_{3/2}|V|0f_{7/2}0d_{3/2}\rangle_{JT}$ with $J=2-5$ and $T=0-1$ have been adjusted in Ref. [22]. The strength of all the two-body matrix elements is scaled by a factor $A^{-0.3}$ in a similar way to the USD interaction. The original strength of the KB and MK interaction is recovered for $A=40$.

We make two kinds of modifications to the above interaction. One concerns the monopole part of interaction, i.e., the (so-called) monopole interaction. At first we mention general properties of the monopole interaction. The monopole interaction between particles in orbits $i$ and $j$ is expressed by the Bansal-French formula [24,25] as

$$H_{ij}^{(mT)}=\sum_{k=i,j}\left\{\frac{a_{kk}}{2}\hat{n}_k(\hat{n}_k-1)+\frac{b_{kk}}{2}\left(\hat{T}_k^2-\frac{3}{4}\hat{n}_k\right)\right\}+a_{ij}\hat{n}_i\hat{n}_j + \frac{b_{ij}}{2}\{(\hat{T}_i+\hat{T}_j)^2-\hat{T}_i^2-\hat{T}_j^2\}. \tag{1}$$

Here, the $\hat{n}_k$ and $\hat{T}_k$ denote the number and isospin operators of the designated orbit, respectively, and the coefficients $a$ and $b$ are given by

$$a_{ij}=\frac{1}{4}(3V_{ij}^1+V_{ij}^0),\quad b_{ij}=V_{ij}^1-V_{ij}^0, \tag{2}$$

$$V_{ij}^T=\frac{\sum_J(2J+1)\langle ij|V|ij\rangle_{JT}}{\Sigma_J(2J+1)},\quad \text{for } T=0,1,$$

where $\langle ij|V|i'j'\rangle_{JT}$ stands for the matrix element of a two-body interaction. Since the angular dependence is averaged out but this interaction still keeps the two-body nature, it should produce effective single-particle energies which depend on both the occupation numbers of various orbits and the isospin structure. We point out that terms proportional to the occupation numbers affect directly effective single-particle energies, once the configuration of a nucleus is given. Moreover, since the calculation of these terms depends only on particle numbers, their effects can be easily magnified for larger particle numbers. The terms containing isospin operators reflect the isospin coupling which is varied as the proton and neutron numbers change. Thus, the monopole interaction plays an important role in the binding energy and the shell gap when the neutron (or proton) number varies. We mention that the coefficients in the monopole interaction are strongly dependent on the isospin: strongly attractive for $T=0$, while rather weak for $T=1$, no matter how attractive or repulsive.

We thus have to pay careful attention to the monopole interaction when we study the single-particle structure. For instance, Poves and Zuker indicated [25] that the Kuo-Brown interaction for the $pf$ shell [21] cannot reproduce the closed-shell structure around $N=28$ owing to a bad monopole property associated with the $0f_{7/2}$. Poves and Zuker adjusted the monopole interaction and changed several matrix elements [25]. They have shown that the modified interaction, called KB3, can describe light $pf$-shell nuclei well [26].

Thus, the effects due to the monopole interaction can be crucial. For $N\simeq Z$ nuclei both the $T=0$ and $T=1$ monopole interactions contribute to a comparable extent. On the other hand, the $T=1$ monopole interaction becomes more dominant over the corresponding $T=0$, in going to unstable nuclei with large neutron excess. In the present case, the O isotopes give us useful information on how to fix the $T=1$ interaction because there are only valence neutrons. The present effective interaction (i.e., USD-KB-MK with the slight modification in [22]) predicts that $^{26}$O is bound for the two-neutron decay by 2.3 MeV, contrary to the experiment [4,6]. This contradiction should be resolved, and indeed can be done by improving the $T=1$ monopole part of the interaction. To be more concrete, the $T=1$ monopole parts should be made more repulsive for the $0d_{3/2}$ and $0f_{7/2}$ orbits. A possible similar modification for $1p_{3/2}$ is omitted just for simplicity. Consequently, the corresponding $T=0$ parts should be more attractive, so that a good fit in $N\sim Z$ stable nuclei can be maintained by cancellation between the $T=0$ and $T=1$ modifications. Thus, one comes up with the modifications as

$$\delta V^{T=1,0}_{0d_{5/2},0d_{3/2}}=+0.30,-0.70\ \text{MeV},$$
$$\delta V^{T=1,0}_{0d_{5/2},0f_{7/2}}=+0.16,-0.50\ \text{MeV}, \tag{3}$$

which means that all the relevant diagonal matrix elements are shifted equally. The modified $T=1$ monopole terms result in only slightly attractive $V^{T=1}_{0d_{5/2},0d_{3/2}}=-0.01$ MeV and $V^{T=1}_{0d_{5/2},0f_{7/2}}=-0.08$ MeV, which are consistent with the general feature of the monopole interaction mentioned above. As shown in Sec. IV, this modification little affects the binding energies of $^{17}$O-$^{24}$O, where neither the $0d_{3/2}$ orbit nor the $pf$ shell is essential in the ground state. But this modification may influence nuclei with $N\geqslant 18$ to some extent. Indeed, we will show later that this modification plays an important role not only for O isotopes, but also for other neutron-rich nuclei.

The other modification concerns the pairing interaction in the $sd$ shell. The USD interaction is designed for the $sd$-shell calculation, where the effects of the $pf$ shell are included implicitly. Now we treat the $pf$ shell more explicitly. We then have to remove certain corrections included empirically in the USD matrix elements. In Ref. [12], this removal was made by the second-order perturbation. In the present study, however, this modification is restricted only to the pairing matrix elements of the $sd$ shell, partly because the major change is considered to be in the pairing matrix elements, and partly because the energy denominators in the perturbation are rather ambiguous. We shift the pairing matrix elements for the $sd$ shell by $\delta G=-0.1$ MeV, where $\langle j'^2|V_{\text{pair}}|j^2\rangle_{JT}=-G/2\sqrt{(2j'+1)(2j+1)}\,\delta_{J0}\delta_{T1}$. This

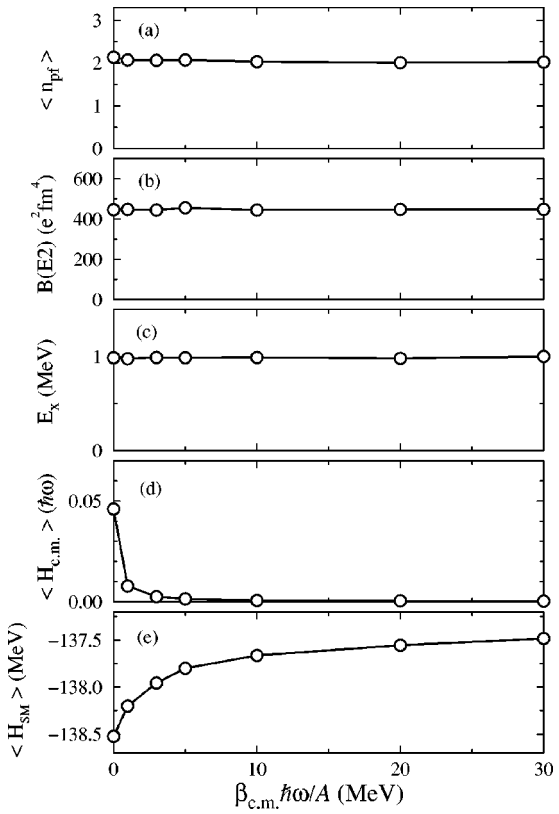


FIG. 1. (a) Neutron occupation number in the $pf$ shell, (b) $B(E2;0_1^+\rightarrow2_1^+)$ value, (c) excitation energy of the $2_1^+$, (d) $\langle H_{\rm c.m.}\rangle$, and (e) $\langle H_{\rm SM}\rangle$ of $^{32}$Mg as a function of $\beta_{\rm c.m.}\hbar\omega/A$.

modification maintains good $2_1^+$ levels of the stable $sd$-shell nuclei to the same extent as the USD interaction.

The single-particle energies (SPE's) are determined so as to reproduce the neutron separation energies and the one-particle spectra of $^{17}$O ($sd$ shell) and $^{41}$Ca ($pf$ shell). The resultant SPE's for the $^{16}$O core are $-3.95$, $-3.16$, 1.65, 3.10, and 3.10 MeV for $0d_{5/2}$, $1s_{1/2}$, $0d_{3/2}$, $0f_{7/2}$, and $1p_{3/2}$, respectively.

## III. OUTLINE OF THE CALCULATION

### A. MCSM calculation

We adopt the latest version of the QMCD method, i.e., phase III [18] to calculate the eigenstates. In phase III, the angular momentum is treated precisely by the projection. The basis states are generated stochastically and searched by monitoring the energy, which is obtained by the diagonalization of the Hamiltonian. In the case of the multishell calculation, the parity is not conserved in the Slater determinant bases in general. Thus in the present study, while monitoring the energies, we project onto the good $M$ (or $J$) and $\pi$, where $\pi$ is the parity, and obtain $M(J)$-compressed bases [18] with parity projection. We basically adopt the $M$-compressed bases when only yrast states are of interest. In the case of calculating non-yrast states, we use the $J$-compressed bases [18].

### B. Treatment of spurious center-of-mass motion

For the calculation beyond one major shell, the spurious center-of-mass motion can be mixed into calculated wave functions, and should be removed to a satisfactory extent. We adopt the prescription of Gloeckner and Lawson [27]. Following this prescription, we replace the Hamiltonian by $H'=H_{\rm SM}+\beta_{\rm c.m.}H_{\rm c.m.}$, where $H_{\rm SM}$ is the original shell-model Hamiltonian. The $H_{\rm c.m.}$ is defined as $H_{\rm c.m.}=\boldsymbol{P}^2/2AM+\frac{1}{2}MA\omega^2\boldsymbol{R}^2-\frac{3}{2}\hbar\omega$, where $\boldsymbol{R}$ and $\boldsymbol{P}$ are the coordinate and momentum of the center of mass. In general, by having a sufficiently large value of $\beta_{\rm c.m.}$, the spurious components become smaller in low-lying states produced by $H'$. We utilize $H'$ in searching favorable basis states and in calculating the wave functions of the final results. The energies and transition matrix elements are calculated from these wave function. Since the value of $\beta_{\rm c.m.}$ should be sufficiently large, we take $\beta_{\rm c.m.}$ as $\beta_{\rm c.m.}/A\hbar\omega=10$ MeV with $\hbar\omega=45A^{-1/3}-25A^{-2/3}$ MeV in the present study.

We examine whether this prescription works well or not. Figure 1 shows the dependence of several physical quantities on $\beta_{\rm c.m.}$ for $^{32}$Mg. One sees that the occupation number, $B(E2)$, and excitation energy are almost constant as a function of $\beta_{\rm c.m.}$. One also finds that the expectation value of $H_{\rm c.m.}$ decreases rapidly toward zero: it becomes less than $10^{-3}\hbar\omega$ for $\beta_{\rm c.m.}/A\hbar\omega=10$ MeV. This means that, since the spurious component carries at least $\langle H_{\rm c.m.}\rangle=2\hbar\omega$, the contamination of the spurious component is less than $1/2\times10^{-3}=0.05\%$, which is quite small. On the other hand, the

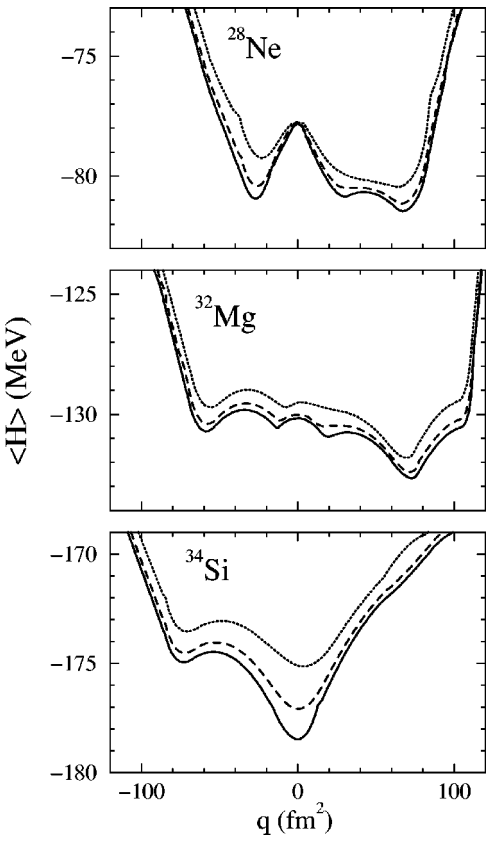


FIG. 2. Potential energy surfaces of $^{28}$Ne, $^{32}$Mg, and $^{34}$Si.. The solid, dashed, and dotted lines denote $I=0$, 2, 4, respectively.

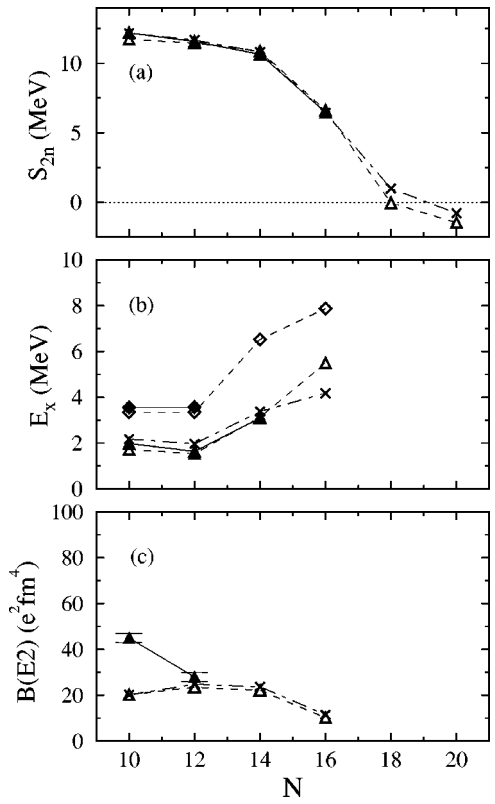


FIG. 3. (a) Two-neutron separation energies, (b) $2_1^+$ (triangles) and $4_1^+$ (diamonds) levels, (c) $B(E2;0_1^+ \rightarrow 2_1^+)$ values of O isotopes. The filled and open symbols mean the experiment and the calculation by the present interaction, respectively. As a comparison, results by the *sd*-shell model calculation with the USD interaction are shown by the crosses. The $2_1^+$ level of $^{22}$O is taken from [33].

binding energy appears to converge rather slowly. As shown in Fig. 1(e), the binding energy still increases by $\sim$200 keV for $^{32}$Mg as $\beta_{\mathrm{c.m.}}/A\hbar\omega$ changes from 10 to 30 MeV. As the binding energy increases likewise for $^{30}$Mg, the two-neutron separation energy varies only weakly as a function of $\beta_{\mathrm{c.m.}}$ at most in the order of magnitude of 10 keV. For the other nuclei, we have obtained the center-of-mass contaminant as small as that of $^{32}$Mg.

### C. Potential energy surface

One of the intriguing issues in the $N\sim20$ region is the competition between the normal configuration and the well-deformed intruder state [28]. The potential energy surface (PES) gives an intuitive picture of the shape coexistence and moreover provides us with useful information on the starting point of the basis generation in the QMCD process (see [29] for the case of $^{56}$Ni). The PES is calculated by the constrained Hartree-Fock method within the shell-model space with the constraints of $\langle J_x\rangle=\sqrt{I(I+1)}$, $\langle Q_0\rangle=q$, and $\langle Q_{\pm1}\rangle=\langle Q_{\pm2}\rangle=0$, where $J_x$ and $Q_\mu$ ($\mu=-2,\ldots,2$) denote the $x$ component of the angular momentum and the mass quadrupole operators, respectively. Here, the value of $I$ is set to be the total angular momentum of the state under consideration, and $q$ is a parameter. Three examples are shown in Fig. 2, and will be discussed in detail in subsequent sections. One can see several local minima, which suggest the shape coexistence in the $N\sim20$ nuclei. One can expect also that in some cases, such as $^{28}$Ne, a strong mixing of several shapes may occur.

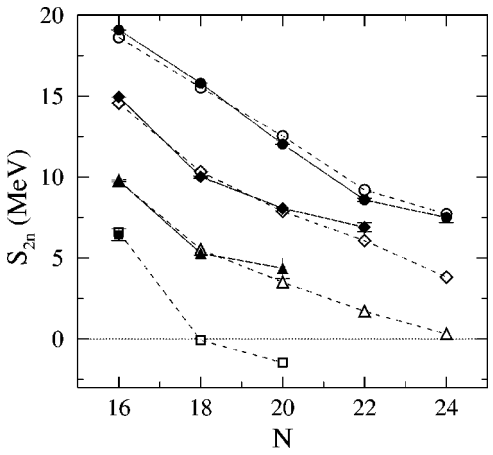


FIG. 4. Two-neutron separation energies in the $N\sim20$ region. The filled (open) squares, triangles, diamonds, and circles denote experimental (calculated) values for O, Ne, Mg, and Si isotopes, respectively. Experimental values are taken from Refs. [30] and [31].

## IV. O ISOTOPES: $T=1$ INTERACTION

We have modified the $T=1$ monopole interaction so as to reproduce the drip line of O isotopes. In this section, we examine the validity of the $T=1$ interaction by calculating some properties of O isotopes. Figure 3 shows the two-neutron separation energies ($S_{2n}$), energy levels, and $B(E2)$ values of O isotopes. The calculation is made by the conventional exact diagonalization method because the shell-model dimension is small. Since we obtain negative $S_{2n}$ values for $^{26}$O ($-80$ keV) and $^{28}$O ($-1.5$ MeV) but a positive value for $^{24}$O, we reproduce the experimental drip line of O isotopes. We have also reproduced the fact that $^{25}$O is unstable for one-neutron emission. In contrast, the $S_{2n}$ of $^{26}$O is 1.0 MeV by the *sd*-shell model with the USD interaction (referred hereafter to as the *sd*-shell model). For $N\leqslant16$ nuclei, both the present and the USD interactions give good descriptions, except for the $B(E2)$ value of $^{18}$O where the $^{16}$O core seems to be still broken to a certain extent. The present effective charge begins to reproduce the experimental $B(E2)$ value for $^{20}$O, implying that the core polarization effect can be well incorporated by the effective charge already for $N=12$. The $2_1^+$ level of $^{24}$O is somewhat different between the *sd*-shell model and the present calculation. This discrepancy is discussed in Sec. V B by using the effective SPE.

## V. RESULTS AND DISCUSSION

### A. Binding energies

Figure 4 shows the two-neutron separation energy ($S_{2n}$). The calculated results are in good agreement with the experiment. We note that the *sd*-shell model, the values of which

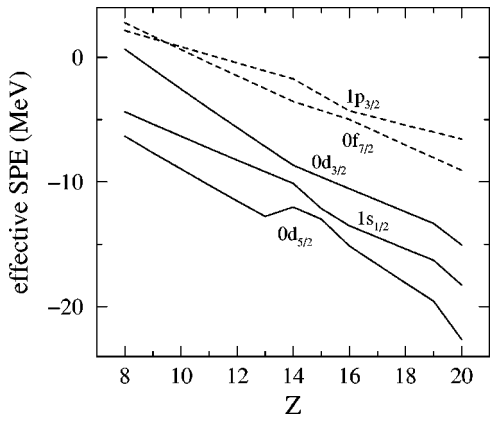


FIG. 5. Effective single-particle energies for $N=20$ isotopes as a function of the proton number.

are not shown in Fig. 4, underestimates the $S_{2n}$ values of $^{30}$Ne and $^{32}$Mg by about 2 MeV. As stated in the previous section, O isotopes with $N>16$ do not exist as bound nuclei. For Ne isotopes, where only even-$A$ isotopes are investigated, our calculation predicts that the heaviest bound nucleus is located at $N=24$ since the calculated $S_{2n}$ values of $^{34,36}$Ne are about $+300$ keV and $-500$ keV, respectively. We would like to emphasize that we have thus succeeded in reproducing the long jump of the drip line in going from $Z=8-10$. We note that the experimental $S_{2n}$ for $^{30}$Ne has been corrected [31] after completion of the present calculation, and that our prediction indeed shows a nice agreement with the new experimental value.

### B. Effective single-particle energy

In order to understand the long jump of the drip line between O and Ne isotopes, the effective (spherical) SPE is of great help. We assume the normal configuration: nucleons are filled in the order of $0d_{5/2}$, $1s_{1/2}$, and $0d_{3/2}$. The effective SPE of one orbit is defined as the one-neutron separation energy of this orbit, where the energy is calculated with the bare SPE's and the monopole interaction whose effects are evaluated by Eq. (1). Figure 5 shows the effective neutron SPE's for $N=20$ isotones. For $Z=8$, the effective SPE's of $0d_{3/2}$, $0f_{7/2}$, and $1p_{3/2}$ are positive and rather close, while the gap between $1s_{1/2}$ and $0d_{3/2}$ is large. Since the deformation of O isotopes is very weak, the $0d_{3/2}$, $0f_{7/2}$, and $1p_{3/2}$ orbits hardly split in the sense of the Nilsson model and remain unbound. Thus, as far as neutrons occupy mainly up to the $1s_{1/2}$ orbit in O isotopes, the nucleus is expected to be bound. Beyond this, no bound O isotopes are expected. The influence of the large gap between $1s_{1/2}$ and $0d_{3/2}$ can be seen in the level structure of $^{24}$O, i.e., this nucleus should be quite spherical with the present interaction. As shown in Fig. 3, the $2_1^+$ level is, in fact, predicted to be at 5.5 MeV, whereas it is at 4.2 MeV by the $sd$-shell model due to a narrower gap between these two orbits.

As the proton number increases from $Z=8$, the effective SPE's go down as a whole. This is due to a strong attractive $T=0$ monopole interaction. We notice also that the gap between the $sd$ and $pf$ shell becomes larger. This is because the proton-neutron interaction is more attractive within the same major shell compared to a proton and a neutron in different shells, as studied with a schematic interaction in Ref. [28]. Since valence protons are in the $sd$ shell, the shell gap at $N=20$ widens with increasing proton number. For Ne and Mg, the gap between $0d_{3/2}$ and $0f_{7/2}$ is still 3.2 and 4.2 MeV, respectively, while the gap ends up with 6.0 MeV for $^{40}$Ca: the $N=20$ closed shell becomes quite stable.

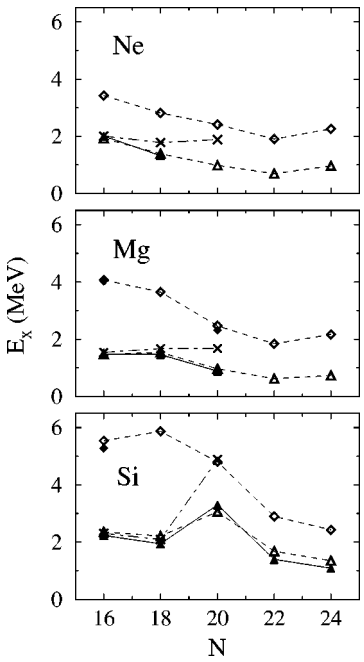


FIG. 6. Yrast levels of Ne (top), Mg (center), and Si (bottom) isotopes. The filled (open) triangles, diamonds are the experimental (calculated) $2_1^+$ and $4_1^+$ levels, respectively. The crosses mean $E_x(2_1^+)$ calculated by the $sd$-shell model.

In the case of Ne, all of the (spherical) $sd$ orbits become bound, but the $0f_{7/2}$ and $1p_{3/2}$ are still unbound in the sense of the effective SPE. These orbits are included in bound many-body states of Ne isotopes due to the coupling to the $sd$-shell orbits. In fact, proton states of Ne isotopes favor deformation, and the neutron shell gap at $N=20$ is still small. The proton-neutron interaction couples these two features. A strong deformation therefore occurs rather easily in Ne isotopes around $N=20$, and additional binding energy is gained. The neutron drip line is thus extended by $\Delta N=8$ in going from O to Ne isotopes.

The calculated drip lines of O and Ne appear to be the same as those given by Caurier *et al.* [14], while a different effective interaction and particle-hole truncations are taken in [14].

### C. Energy levels and $B(E2)$ values

We show the levels in Fig. 6 and the $B(E2)$ values in Fig. 7. The $E2$ matrix elements are calculated with the effective charges $e_p=1.3e$ and $e_n=0.5e$, which are the same as those adopted in the $sd$-shell model [20]. It is pointed out that the $E2$ effective charges should remain basically unchanged in going from the $sd$-shell to the $sd+pf$ shell calculations.

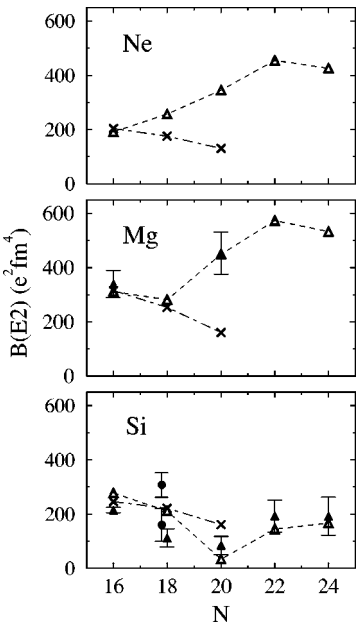


FIG. 7. $B(E2;0_1^+ \rightarrow 2_1^+)$ values of Ne (top), Mg (center), and Si (bottom) isotopes. The filled (open) triangles mean experimental (calculated) values, while the crosses are those obtained by the $sd$-shell model. For $^{32}$Si, previously measured quantities [37,38] are also shown by circles.

#### *1.* Ne *isotopes*

A recent experiment at GANIL shows that the $2_1^+$ levels $[E_x(2_1^+)]$ of $^{26}$Ne [32,33] and $^{28}$Ne [33] are at $2010 \pm 30$ and $1320 \pm 30$ keV, respectively. The $E_x(2_1^+)$ of $^{26}$Ne is similar to the result of the $sd$-shell model. The $sd$-shell model predicts that $E_x(2_1^+)$ remains almost constant from $N=16$ to 20. On the contrary, the experimental value of $E_x(2_1^+)$ for $^{28}$Ne drops considerably [33], implying that the $N=20$ closed-shell structure is weakened already at $N=18$ for Ne. The present calculation indeed reproduces this $2_1^+$ level. To understand the situation more transparently, we analyze the PES of $^{28}$Ne in Fig. 2. One can see two local minima on the prolate side, namely $\sim 30$ and $\sim 70$ fm$^2$. The former state corresponds to a $\gamma$-unstable deformed state formed primarily by $sd$-shell configurations, while the latter is dominated by the $2p4h$ excitations from the $N=20$ core. Since these two minima are nearly degenerate, a strong mixing can occur. The result by the MCSM clearly shows this mixing: the neutron occupation number in the $pf$ shell is about one for the ground state of $^{28}$Ne, whereas it is only $<0.1$ for $^{26}$Ne. The occupation in the $pf$ shell becomes larger as the spin increases. This strong mixing is consistent with Fig. 5: the gap between the $0d_{3/2}$ and the $pf$ shell is only about 3 MeV for Ne isotopes, producing the present mixed wave functions. This narrow gap is not so relevant for $N \leqslant 16$, where the neutrons occupy mainly orbitals up to $1s_{1/2}$ or below.

For Ne with $N \geqslant 20$, large prolate deformations are obtained. We predict that the largest deformation occurs at $N=22$. As shown in Fig. 8, a considerable intruder component is involved in Ne isotopes for $N \geqslant 18$.

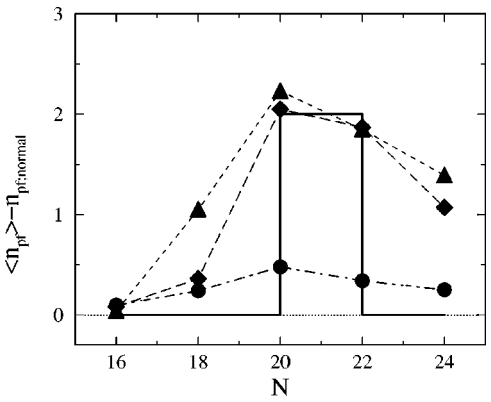


FIG. 8. Average number of neutrons in the $pf$ shell subtracted by the corresponding number in the normal (i.e., filling) configuration. The triangles, diamonds, and circles stand for the values of Ne, Mg, and Si isotopes, respectively. The solid line denotes the corresponding value of Ne and Mg isotopes as predicted by the ''island of inversion'' of [11].

#### *2.* Mg *isotopes*

Figure 6 shows that the experimental $E_x(2_1^+)$ values of $^{28,30}$Mg are consistent with the $sd$-shell model. The MCSM calculation confirms it. The neutron occupation number in the $pf$ shell is only about 0.1 for the $0_1^+$ of $^{28}$Mg. It increases for $^{30}$Mg, but the normal configuration still dominates the ground state as shown in Fig. 8. We have investigated the $0_2^+$ state of $^{28}$Mg, since it is known experimentally. The observed $0_2^+$ state lies at 3.9 MeV [34], while we have obtained it at 4.0 MeV.

The Mg isotopes with $N=20$, 22, and 24 are strongly prolate deformed. The intruder configuration dominates the ground state for $N=20$ and 22 as well as $^{30,32,34}$Ne, while it becomes less dominant for $N=24$. The $E_x(2_1^+)$ and $B(E2)$ values of $^{32}$Mg are in agreement with the experimental results [2,3]. Recently, a $\gamma$ line at 1470 keV in $^{32}$Mg has been observed by Azaiez *et al.* in coincidence with 885 keV ($2_1^+$ to $0_1^+$), and its quadrupole nature is being studied [33]. If this $\gamma$ line corresponds to the $E2$ transition from the $4_1^+$ to $2_1^+$, $E_x(4_1^+)/E_x(2_1^+)$ is 2.66. In the MCSM calculation, this ratio turns out to be 2.55.

#### *3.* Si *isotopes*

For Si isotopes, the intruder configurations are not dominant in the ground states. As a result, the $B(E2)$ values from the ground state are suppressed in comparison to the cases of Ne and Mg. The $E_x(2_1^+)$ and $B(E2)$ values have been measured recently up to $N=24$ [35,36]. They are in agreement with our results except for the $B(E2)$ of $^{32}$Si. The calculated $B(E2)$ value of $^{32}$Si is about twice larger than a recently measured one [36], but is consistent with a previously measured one [37]. The obtained deformation of $^{32}$Si is consistent with the result by the $sd$-shell model, since our interaction is based on the USD and the intruder component is rather small.

We discuss the deformation of Si isotopes. In Fig. 5 we find that the effective neutron gap between the $0d_{3/2}$ and

$0f_{7/2}$ is 5.1 MeV for $^{34}$Si, which is larger than that of Ne and Mg. Furthermore, for Si isotopes the $0d_{5/2}$ is fully occupied by protons in the normal filling, and the $0d_{5/2}$ sub-shell closure for protons is rather stiff because the effective proton gap between $0d_{5/2}$ and $1s_{1/2}$ is 6.7 MeV. Thus, much weaker deformation is expected for Si than for Ne and Mg. The stiffness of the $0d_{5/2}$ subshell closure gives rise to an interesting structure in $^{34}$Si. The ground state of $^{34}$Si is dominated by the closed $\pi(0d_{5/2})^6\nu(sd)^{12}$ configuration, which produces $q=0$ in the PES of Fig. 2. In order to construct excited states, the $\pi(0d_{5/2})^6\nu(sd)^{12}$ core must be broken. There are two candidates of the $2_1^+$ state in the PES: $q\sim 0$ fm$^2$ and $q\sim -70$ fm$^2$. The former is dominated by the $sd$-shell configuration, while the main component of the latter is the neutron $2p2h$ excitation from the $sd$-shell core. In the present calculation, the $2_1^+$ is dominated by the $2p2h$, because the breaking of the proton $0d_{5/2}$ core requires even more energy. Thus, the $B(E2;0_1^+\rightarrow 2_1^+)$ value of $^{34}$Si is more suppressed than in the $sd$-shell model, since the dominant configurations of the $0_1^+$ and $2_1^+$ are different. Note that the $2_1^+$ level is much higher in the $sd$-shell model than in the present calculation. The spectroscopic quadrupole moment of the $2_1^+$ is calculated to be 16 $e$ fm$^2$, which means a large oblate deformation. The present result basically has the same feature as the truncated shell-model calculations [14,36]. In Ref. [14] by Caurier *et al.*, the $0p0h$ and $2p2h$ configurations are not mixed basically. For $^{34}$Si, the ground state appears to be in the $0p0h$ configuration, whereas the $2_1^+$ is the $2p2h$. Consequently, the $E2$ transition between them is forbidden. To remedy this apparent contradiction to experiment, the two configurations are mixed for $^{34}$Si in Ref. [14], producing a reasonable $E2$ transition. From the PES, the energy difference between these two configurations can be estimated to be 3.5 MeV for $I=0$. We point out that the energy difference is smaller in many other nuclei around $N=20$, where the mixing may play even more significant roles.

## VI. MIXING AND INVERSION OF NORMAL AND INTRUDER CONFIGURATIONS

The region where the $2p2h$ configuration dominates the ground state over the $0p0h$ is often referred to as the ''island of inversion'' [11]. In the previous shell-model calculations [11,14], the authors discussed the extent of the island by comparing the energies of both configurations. They showed that the island consists of several Ne, Na, and Mg nuclei with $N\geqslant 20$. In the present calculation, the mixing and inversion among various configurations are included in a natural way. In this section, we discuss, rather in detail, how the mixing occurs.

In Fig. 8, we present the number of neutrons excited from the $sd$ to $pf$ shell for the ground state, together with the corresponding value as predicted by the ''island of inversion'' of [11]. Some nuclei cannot be clearly classified whether they correspond to the $0p0h$ or $2p2h$ configuration in the present calculation. Figure 8 may seem to display that $^{32}$Mg is composed of almost pure $2p2h$ configuration from the $sd$-shell core. We, however, point out that the ground state of $^{32}$Mg by the pure $2p2h$ configuration loses energy by $\sim 200$ keV compared to the calculation where the $0p0h$ configuration is included too. The binding energy obtained by the MCSM is even lower by $\sim 500$ keV than this $0p0h+2p2h$ truncation, due to the mixing beyond the $2p2h$ configuration. The pure $2p2h$ truncation is taken in [14], but there is about 700 keV energy gain in the full calculation with the present interaction.

The neutron occupation number excited to the $pf$ shell peaks at $N=20$ for all isotope chains. At $N=20$, the $0p0h$ states gain energy only a little from the deformation, so that the intruder configuration come down more relative to the normal configuration in comparison to the other isotopes of $N\neq 20$. But for Si the intruder is not dominant even at $N=20$ as mentioned above.

We discuss Ne and Mg, paying attention to their similarity and difference. There is little intruder component at $N=16$ for both isotopes. Here, the Fermi surface lies at the $1s_{1/2}$ orbit, which is far from the $pf$ shell. As $N$ increases over $N=16$, the $2p2h$ configuration mixes apparently, and it eventually becomes dominant at $N=20$ for both. The occupation number in the $pf$ shell reaches about 2 for $N=20$. At $N=18$, however, there is a significant difference between Ne and Mg. Namely, for $^{28}$Ne the $2p2h$ configuration already occupies the ground state wave function up to about half, while its occupation is still small for $^{30}$Mg. As shown in Fig. 5, the energy gap between the $0d_{3/2}$ and $pf$ shell is smaller by 1.0 MeV in Ne than in Mg. Thus, this gap has a very direct impact on the extent of the mixing for nuclei in the transitional region. Experimentally, this mixing appears to be reflected by a different behavior of the $2_1^+$ level of Ne and Mg in the transition from $N=16$ to 18: the observed $2_1^+$ level comes down for $^{28}$Ne, while it remains almost unchanged for $^{30}$Mg. If there were no mixing, it would stay almost constant also for $^{28}$Ne, as is the case for $^{30}$Mg. We predict that the $B(E2)$ value of $^{28}$Ne increases from $N=16$ to 18 due to the mixing. The $B(E2)$ of $^{30}$Mg is predicted to decrease similarly to the $sd$-shell model.

Over $N=20$, the intruder configurations gradually become less dominant for Ne and Mg. They, however, do not vanish as quickly as expected by the ''island of inversion'' of [11,14]. Our result shows that the intruder configuration cannot be negligible even at $N=24$, while in the previous calculations [11,14] $N=24$ does not belong to the island.

Nucleons excited from the $sd$ to the $pf$ shell are distributed over the two $pf$ orbits. For example, the ratio between the occupation numbers of the $0f_{7/2}$ and $1p_{3/2}$ is about 6:1 for $^{32}$Mg, while about 3:1 for $^{30}$Ne. Thus, considerable mixing occurs between the $0f_{7/2}$ and $1p_{3/2}$. Since these two orbits are $\Delta l=\Delta j=2$, they are easily coupled by the quadrupole deformation. On the other hand, holes excited from the $sd$ to the $pf$ shell are mainly composed of the $0d_{3/2}$.

## VII. SUMMARY

In this paper, we have studied the structure of $N\sim 20$ unstable even-even nuclei from O to Si within the Monte Carlo shell model based on the QMCD method. Except for O iso-

topes, there have been no conventional shell-model calculations where all particle-hole configurations are mixed on an equal footing. We have succeeded in reproducing the two-neutron separation energies, the excitation energies, and the $B(E2)$ values systematically, and a number of predictions have been presented. We emphasize that no parameters were adjusted in calculating these quantities for the Ne, Mg, and Si isotopes investigated in this paper. The interplay between the $T=1$ and $T=0$ monopole interactions has been shown to be quite essential to produce various intriguing properties in these unstable nuclei, including the drip line of O isotopes and the recent observation of the excitation energy of $^{28}$Ne. It turned out that, the drip line of O isotopes is at $^{24}$O, while that of Ne isotopes is extended to $^{34}$Ne. This is due to the above interplay of the monopole interactions and the deformation of Ne isotopes varying as the neutron number changes. We note that, because of variable mixing between the normal $(0p0h)$ and intruder $(2p2h$ and more) configurations, the boundary of the ''island of inversion'' may be more complex than expected in [11], and, in fact, does not appear to be very definite. On the other hand, the present study confirms that, with such full calculations, the basic concept of the ''island of inversion'' can still make sense particularly for its primary region. Many of the above features can be studied only through a calculation with full mixing between normal and intruder configurations. Our result indicates that the intruder state plays a very important and subtle role in moving over $N=20$.

## ACKNOWLEDGMENTS

We acknowledge Dr. N. Fukunishi for discussions at the early stage of our research. We thank Professor A. P. Zuker and Dr. H. Sakurai for useful comments, and thank Dr. F. Azaiez, Professor W. Mittig, and Dr. F. Sarazin for valuable discussions on their recent data. We are grateful to Professor A. Gelberg for reading the manuscript. The conventional shell-model calculations are obtained using OXBASH [39]. Computations have been carried out partly by the Alphleet computer system of RIKEN. This work was supported in part by Grant-in-Aid for Scientific Research (B) (No. 08454058) and (A)(2)(10304019) from the Ministry of Education, Science and Culture.

[1] C. Thibault *et al.*, Phys. Rev. C **12**, 644 (1975).
[2] C. Détraz *et al.*, Phys. Rev. C **19**, 164 (1979); D. Guillemaud-Mueller *et al.*, Nucl. Phys. **A426**, 37 (1984).
[3] T. Motobayashi *et al.*, Phys. Lett. B **346**, 9 (1995).
[4] D. Guillemaud-Mueller *et al.*, Phys. Rev. C **41**, 937 (1990).
[5] O. Tarasov *et al.*, Phys. Lett. B **409**, 64 (1997).
[6] M. Fauerbach *et al.*, Phys. Rev. C **53**, 647 (1996).
[7] H. Sakurai *et al.*, Phys. Lett. B **448**, 180 (1999).
[8] H. Sakurai *et al.*, Phys. Rev. C **54**, R2802 (1996).
[9] X. Campi, H. Flocard, A. K. Kerman, and S. Koonin, Nucl. Phys. **A251**, 193 (1975).
[10] A. Poves and J. Retamosa, Phys. Lett. B **184**, 311 (1987); Nucl. Phys. **A571**, 221 (1994).
[11] E. K. Warburton, J. A. Becker, and B. A. Brown, Phys. Rev. C **41**, 1147 (1990).
[12] N. Fukunishi, T. Otsuka, and T. Sebe, Phys. Lett. B **296**, 279 (1992); T. Otsuka and N. Fukunishi, Phys. Rep. **264**, 297 (1996).
[13] S. E. Koonin, D. J. Dean, and K. Langanke, Annu. Rev. Nucl. Part. Sci. **47**, 463 (1997).
[14] E. Caurier, F. Nowacki, A. Poves, and J. Retamosa, Phys. Rev. C **58**, 2033 (1998).
[15] M. Honma, T. Mizusaki, and T. Otsuka, Phys. Rev. Lett. **75**, 1284 (1995).
[16] T. Mizusaki, M. Honma, and T. Otsuka, Phys. Rev. C **53**, 2786 (1996).
[17] M. Honma, T. Mizusaki, and T. Otsuka, Phys. Rev. Lett. **77**, 3315 (1996).
[18] T. Otsuka, M. Honma, and T. Mizusaki, Phys. Rev. Lett. **81**, 1588 (1998).
[19] For a review, T. Otsuka, T. Mizusaki, and M. Honma, J. Phys. G **25**, 699 (1999).
[20] B. A. Brown and B. H. Wildenthal, Annu. Rev. Nucl. Part. Sci. **38**, 29 (1988).
[21] T. T. S. Kuo and G. E. Brown, Nucl. Phys. **A114**, 241 (1968).
[22] E. K. Warburton *et al.*, Phys. Rev. C **34**, 1031 (1986).
[23] D. J. Millener and D. Kurath, Nucl. Phys. **A255**, 315 (1975).
[24] R. K. Bansal and J. B. French, Phys. Lett. **11**, 145 (1964).
[25] A. Poves and A. Zuker, Phys. Rep. **70**, 235 (1981).
[26] E. Caurier, A. P. Zuker, A. Poves, and G. Martínez-Pinedo, Phys. Rev. C **50**, 225 (1994); G. Martínez-Pinedo, A. P. Zuker, A. Poves, and E. Caurier, *ibid.* **55**, 187 (1997).
[27] D. H. Gloeckner and R. D. Lawson, Phys. Lett. **53B**, 313 (1974).
[28] K. Heyde and J. L. Wood, J. Phys. G **17**, 135 (1991).
[29] T. Mizusaki, T. Otsuka, Y. Utsuno, M. Honma, and T. Sebe, Phys. Rev. C **59**, R1846 (1999).
[30] G. Audi *et al.*, Nucl. Phys. **A624**, 1 (1997).
[31] F. Sarazin *et al.*, in *Proceedings of the XXXVII International Winter Meeting on Nuclear Physics*, Bormio, 1999.
[32] A. Reed (private communication).
[33] F. Azaiez *et al.*, in *Proceedings of the International Conference ''Nuclear Structure 98''*, Gatlinburg, 1998.
[34] P. M. Endt, Nucl. Phys. **A521**, 1 (1990).
[35] P. Baumann *et al.*, Phys. Lett. B **228**, 458 (1989).
[36] R. W. Ibbotson *et al.*, Phys. Rev. Lett. **80**, 2081 (1998).
[37] J. G. Pronko and R. E. McDonald, Phys. Rev. C **6**, 2065 (1972).
[38] G. Guillaume *et al.*, Nucl. Phys. **A227**, 284 (1974).
[39] A. Etchegoyen *et al.*, MSU-NSCL Report No. 524, 1985.